Original Paper

Alexander Ulanovsky

Absorbed doses in tissue-equivalent spheres above radioactive sources in soil

Alexander Ulanovsky (✉)
Institute for Radiation Protection, Helmholtz Zentrum München – German Research Center for Environmental Health, Ingolstädter Landstraße 1, Neuherberg, Germany
E-Mail: ulanovsky@helmholtz-muenchen.de
Tel.: +49-89-3187-4113
Fax: +49-89-3187-3363

Abstract Doses due to external exposure of terrestrial biota are assessed using differential air kerma from radioactive sources in soil and energy-dependent 'absorbed dose-per-air kerma' conversion factors computed for spherical tissue-equivalent bodies. The presented approach allows computing average whole body absorbed dose for terrestrial organisms with body masses from 1 mg to 1 ton located at heights from 10 cm to 500 m above ground. Radioactive sources in soil emitting photons with energies from 10 keV to 10 MeV have been considered. Interpolation of the computed quantities over source energy, body mass, and height above ground results in plausible estimates of whole body average absorbed doses for non-human terrestrial biota from gamma-radiation emitted by any radionuclides in contaminated terrain.

Keywords: Absorbed dose, external exposure, radionuclides in soil, non-human biota

Introduction

Calculation of doses due to external exposure of terrestrial animals and plants represents one of the existing gaps of contemporary dosimetric methodology of the International Commission on Radiological Protection (ICRP) for non-human biota. The methodology used by ICRP to compute dose conversion coefficients (DCC) for non-human biota (ICRP 2008a) is largely the same as implemented in the ERICA Tool (Brown et al. 2006). That is, the DCC for external exposure of terrestrial animals have been based on results of Taranenko et al. (2004), which included terrestrial animals with masses in the range from 0.17 g to 550 kg on top of the ground interface, and birds of mass from 35 g to 2 kg at heights above ground in the range from 0 to 10 m. Contrary to this, internal and external exposure DCC for aquatic biota can be computed in the range of masses from 10^{-6} to 10^{3} kg accounting for effects of body shape (Ulanovsky and Pröhl 2006). Moreover, ignoring minor differences in radiation scattered back from water or air surrounding the organism, internal exposure DCC for terrestrial organisms can be also estimated by the method developed for aquatic biota (Ulanovsky and Pröhl 2008; Ulanovsky et al. 2008). That is, range of applicability of the current external exposure DCCs for terrestrial organisms does not match that for aquatic ones or even one for internal exposure DCC for terrestrial organisms, thus leaving inconsistency in the existing recommended dosimetric approach.

External exposure due to radioactivity in soil has been systematically studied for several decades with results presented elsewhere (see e.g. Beck and de Planque 1968; Eckerman and Ryman 1994; Saito and Jacob 1995; ICRP 1996, 2011). Not surprisingly, most studies were supporting either external exposure assessment for humans in radioactively contaminated environment or providing important parameters for *in-situ* gamma-spectrometry. Publications of the ICRP devoted to human external exposure (ICRP 1996, 2011) are focused on providing organ-specific dose or effective dose conversion coefficients for simple idealized irradiation geometries. Such DCCs are used for dose assessment and radiation protection of humans in cases of occupational, medical, or accidental exposures (ICRP 2007).

Assessment of external exposures of non-human biota in their natural environments is a more complicated task, due to extreme variability and diversity of non-human biota. An attempt of developing a common technique for dose assessment for various organisms can be successful only if the modelling techniques account for the main principal features and omit

or ignore less significant ones. In other words, use of simple albeit plausible and robust models is the main practical method to deal with existing bio-diversity.

In the course of the present study the dose response of diverse terrestrial animals to external radiation was evaluated by Monte Carlo simulation of radiation transport in animals and their habitats. The computed dataset has created a grid for interpolation of dose response for body mass, height above ground, source energy, thus providing a basis for computation of external exposure DCC for arbitrary values within considered ranges and for any radionuclide of interest. Particularly, the new dataset extends mass range to be compatible with already used for aquatic biota and implemented in the ICRP methodology (ICRP 2008a), considerably extends range of heights and masses for exposure above ground, adds the new uniform source in soil, which together with planar source indicates range of DCC variability due to variation of radioactivity distribution in soil. Such extensive computational work became feasible due to factorization of biota external doses into source-specific air kerma above contaminated terrain and absorbed dose-per-air kerma response of biological objects to external exposure, which have been estimated independently by most appropriate and effective Monte Carlo techniques.

Materials and methods

Radioactive sources in soil

Radioactive photon-emitting sources have been modelled for an idealized 'infinite' plain and homogeneous terrain. Specifically, the computational model includes a homogeneous 10-m-thick circular soil layer and 1-km-thick air layer above the soil surface, to allow calculation of exposure from skyshine. The model's radius has been set to 5 km, which corresponds to more than eight mean free paths in air for photons with energies up to 10 MeV. The densities and elemental compositions of air and soil have been selected as in Eckerman and Ryman (1993). The elemental compositions are shown in Table 1. Density of air, 1.205 kg m^{-3}, and its elemental composition correspond to air at 20°C and normal atmospheric pressure with 40% relative humidity. Soil has been modelled as a homogeneous layer of density 1600 kg m^{-3}.

[Table 1 is about here]

Three types of depth distribution for radioactive sources have been modelled. The first one, so-called 'effective' planar source, is an infinite isotropic plane source at depth 0.5 g cm^{-2}, which is known to represent a radiation field of freshly deposited radioactivity, accounting for effects of the ground surface roughness and initial migration (Jacob and Paretzke 1986).

The second modelled source is a volume source uniformly distributed in the upper 10-cm-layer of soil. This source results in radiation fields similar to those due to aged radioactive depositions, where radioactive materials have already been significantly migrated downwards and appear distributed in depth of the upper soil. Apparently, the uniform distribution in soil depth is an approximation, which does not account for more subtle effects of radionuclide migration resulting in various shapes of depth distributions, which may be described by exponential or Lorentzian shapes (see e.g. Hillmann et al. 1996; Saito et al. 2012). However, plausibility of depth distribution modelling is more important in certain applications related to in-situ gamma-spectrometry, while total dose in air, created by both direct and scattered radiation, is less sensitive to variations of depth distributions (see e.g. Beck and de Planque 1968). It is not unlikely, that variability of depth profiles due to migration, weathering, wash-out, covering by clean materials, and other effects, results in a situation where the uniform depth distribution can be regarded as the most appropriate approximation for assessing dose rates above contaminated ground.

The third modelled source is a uniform distribution to infinite depth. A source of this type is applicable to model the distribution of naturally-occurring radioactive materials (NORM) in soil.

Absorbed dose rates above ground interface

Free-in-air kerma K_{air} (ICRU 2011) at height H above radioactively contaminated terrain with photon sources of energy E_x can be expressed as follows:

$$K_{air}\left(E_x,H\right)=\int_0^{E_x}\frac{\mu_{tr}}{\rho}\left(E\right)E\frac{d\Phi}{dE}\left(E,E_x,H\right)dE=\int_0^{E_x}K\left(E,E_x,H\right)dE\,, \qquad (1)$$

where $\frac{\mu_{tr}}{\rho}(E)$ is the mass-energy transfer coefficient ($cm^2\ g^{-1}$), $\frac{d\Phi}{dE}(E,E_x,H)$ is the angle-integrated differential photon fluence per source particle ($cm^{-2}\ \gamma^{-1}\ MeV^{-1}$) and, correspondingly, $K(E,E_x,H)$ is the differential air kerma per source particle ($Gy\ \gamma^{-1}\ MeV^{-1}$).

Absorbed dose in an organism with body mass *M* located above contaminated soil can be expressed via differential air kerma at the same location and organism-specific energy-dependent dose response:

$$D(E_x,H,M)=\int_0^{E_X} K(E,E_x,H)R(E,M)dE\,, \qquad (2)$$

where the dose response *R(E,M)* denotes a ratio of mean absorbed dose in the organism of mass *M* and free-in-air kerma at the same location due to monoenergetic photons incident on the organism's body surface.

In general, the conversion factor *R* depends on energy and angular distribution of an incident photon fluence as well as on mass and geometric shape of an organism. In the present study, the dosimetric endpoint is the average absorbed dose in the whole body. Therefore, subtle effects of anisotropic angular dependence of dose response are not accounted for and angular-integrated kerma spectra are used. Correspondingly, biological objects above ground are modelled as tissue-equivalent spheres and their dose response per air kerma is computed for isotropic photon fields.

Use of simplified spherical shapes and isotropic radiation fields can also be justified by the fact that the average absorbed dose in the whole body of terrestrial organisms is effectively averaged in radiation fields created by photon-emitting radionuclides in the environment, due to the movement of the organisms. That is, the effect of body shape and anisotropy of gamma-radiation is less significant compared to other factors, like distance to source, source distribution, and time of exposure. If the mean free paths of incident photons in tissue are similar or larger than the dimensions of a target volume, then the absorbed dose is proportional to the mean chord length in this volume. Note that among convex bodies the mean chord length is maximal for spheres (see e.g. eq. (2.112) in Bell and Glasstone 1970). Therefore, dose coefficients for spherical bodies can be regarded as conservative estimates of those for bodies with more realistic shapes in many realistic situations of external exposure to gamma-radiation.

The four-component soft tissue of ICRU (1989) has been taken to represent the organism's body. The spheres are uniform with density 1 g cm^{-3}, and no skeleton, air-filled cavities or organs have been considered. The spheres' masses have been selected to provide a reasonable grid for interpolation and to comply with the existing ICRP methodology (ICRP, 2008a), i.e. 10^{-6}, 10^{-5}, 10^{-4}, 10^{-3}, 10^{-2}, 0.1, 1, 10, 10^{2}, 10^{3} kg.

Absorbed doses in the body have been estimated using coupled photon-electron transport and analogue energy-deposition estimators (tally *F8, according to MCNP terminology). Photon and electron energy cut-offs have been taken equal to 1 and 10 keV, respectively

Results

Differential air kerma

Differential air kerma rates (spectra) have been simulated by Monte Carlo method using the MCNP code (LANL X-5 Monte Carlo Team 2003). The spectra have been computed in group representation as integral air kerma (track-length-based estimator of energy deposition) per unit source strength in 30 energy bins, equally spaced in log-scale from 10 keV to 10 MeV (Eq. 3)

$$\tilde{K}_i(E_x,H) = \int_{\Delta_i} K(E,E_x,H)\,dE, \quad \text{where } \Delta_i = E_i - E_{i-1}, \quad E_0 \equiv 0\,. \tag{3}$$

Use of air kerma spectra in the group form allows re-writing Eq. (2) as follows:

$$D(E_x,H,M) = \sum_i \frac{\tilde{K}_i(E_x)}{\Delta_i} \int_{\Delta_i} R(E,M)\,dE\,. \tag{4}$$

Introducing the average absorbed dose-per-air kerma response in the i^{th} energy bin

$$\bar{R}_i(M) = \frac{1}{\Delta_i} \int_{\Delta_i} R(E,M)\,dE\,, \tag{5}$$

one finally gets Eq.(2) in group form (Eq. 6):

$$D(E_x, H, M) = \sum_i \tilde{K}_i(E_x, H)\bar{R}_i(M), \quad (6)$$

where average absorbed dose in the whole body is represented as a sum over energy groups of the two independently computed functionals.

Uncertainty due to discretization and use of dosimetric quantities in group representation is relatively low, because integrals of air kerma values within energy bins have been computed exactly by Monte Carlo method and, as it will be shown later, the absorbed dose-per-air kerma response is a smooth function of photon energy and its variation within the limits of an energy bin can be regarded as small.

Air kerma spectra have been computed for 12 heights ranging from 0.1 to 500 m above ground interface, namely, 0.1, 0.2, 0.5, 1, 2, 5, 10, 20, 50, 100, 200, 500 meters. Examples of computed air kerma spectra at various heights are shown for a 10 MeV plane source in Fig. 1 and for a 1 MeV uniform 10-cm-thick volume source in Fig. 2.

[Fig. 1 is about here]

[Fig. 2 is about here]

The infinitely thick source in soil has been modelled as a source uniformly distributed in the upper soil layer down to a depth equal to six mean free paths of the source photons in soil.

Here, air kerma spectra have been computed for a number of fixed values of source energy and detector heights above ground. To use these spectra for calculation of dose coefficients for arbitrary source energies and heights, the following technique has been used to interpolate the spectra. For source energy E within limits of i^{th} energy bin, the two spectra pre-calculated for energies E_{i-1} and E_i have been transformed along energy axis (extracted and shrunk, correspondingly). Then, a weighted sum of both spectra has been calculated, thus resulting in an estimate of spectrum for the given source energy E. The latter can be further log-linearly interpolated for height in every bin, thus resulting in the estimated differential air kerma spectrum for the given photon source energy and organism's height above ground.

In Fig. 3, air kerma spectra from plane and 10-cm-thick volume sources normalized per equal surface source strength are compared, for 0.5 MeV photons and heights of 1 and 500 m.

The figure shows that the effect of height above ground is much more pronounced than that of variation of specific activity distribution in the upper soil layer.

[Fig. 3 is about here]

Absorbed dose-per-air kerma ratios

Absorbed dose-per-air kerma ratios have been computed using Monte Carlo simulation of radiation transport in tissue-equivalent spheres in air irradiated by a monoenergetic isotropic photon field. Energies of source photons have been selected to match energy groups of the air kerma spectra, thus each dose response consists of 31 energy values, equally spaced on logarithmic scale.

The computed response (see Fig. 4) is a smooth function of log-transformed mass and energy, which makes interpolation convenient. Namely, log-linear cubic spline interpolation of *R(E,M)* for mass values results in an estimated response function for the given body mass *M* as a function of energy. The latter can also be approximated by a cubic spline for energy in log-linear scale, and the constructed cubic spline can analytically be integrated in the appropriate energy intervals resulting in bin-averaged values of the absorbed dose-per-air kerma response, $\bar{R}_i$ (see eq.(5)).

[Fig. 4 is about here]

The absorbed dose-to-air kerma response depends on energy of source photons and on body mass. As seen in Fig. 4, the strong attenuation of low-energy photons in massive bodies leads to a reduction of the average absorbed dose when compared to free-in-air kerma. This is the case of 'opaque' bodies, which are non-transparent to the specific radiation. A similar reduction of absorbed dose can be observed in the opposite case of low body masses and high energies of source photons; this is the case of bodies 'transparent' to radiation of the given energy. It is also worth noting that in the range of source energies from approximately 20 keV to 2 MeV and for bodies with masses from approximately 1 g to 100 kg the absorbed dose-to-air kerma ratio does not vary much and shows values between 0.8 and 1.15, thus indicating that air kerma can serve as a plausible surrogate for the average whole body absorbed dose.

221

222 Doses of external exposure due to sources in soil

223 Independently calculated air kerma spectra and absorbed dose-per-air kerma ratios are
224 convoluted together to obtain dose conversion coefficients for external exposure of terrestrial
225 organisms. In this way, average absorbed dose rates per unit activity concentration can be
226 obtained for body masses ranging from 10^{-6} to 10^{3} kg, at heights above ground from 10 cm to
227 500 m, and for sources emitting photons with energy from 10 keV to 10 MeV. Providing
228 detailed tables for various animals, exposure conditions, and for hundreds of nuclides of
229 radiological interest is not the goal of the present paper, but this can be done using the
230 presented approach and a computer program, which can address any combination of the
231 parameters.

232 In the present work, DCCs for a limited set of radionuclides were calculated and are
233 presented to illustrate the main tendencies and to facilitate comparisons with other estimates.
234 Radionuclides of anthropogenic origin are considered with two types of sources: 'effective'
235 planar and 10-cm-thick volume sources. The DCCs for anthropogenic radionuclides were
236 computed for several body masses and heights above ground, for the planar source (Table 2)
237 and for the volume source in the upper 10 cm of soil (Table 3). Radionuclide emission data
238 were taken from (ICRP 2008b). For some nuclides in the tables, the DCCs include
239 contribution from radioactive progeny. Relative activity of the progeny was estimated as ratio
240 of the time-integrated activities of a daughter and the parent nuclides. Integration time has
241 been selected differently: for the effective planar source typical for 'fresh' depositions the
242 integration period has been taken 15 days, while for the volume 'aged' source – 1 year.

243 [Table 2 is about here]

244 [Table 3 is about here]

245 The DCC for radionuclides of primordial origin, NORM, have been computed for the
246 infinitely deep uniform source (Table 4) for the main uranium and thorium series as well as
247 for ^{40}K. Relative activities of radioactive progeny in the ^{235}U-, ^{238}U- and ^{232}Th-series to that of
248 their parents have been calculated based on the assumption of secular equilibrium.

249 [Table 4 is about here]

Discussion

Representation Eq. (2) of absorbed dose in the whole body as a product of differential air kerma and absorbed dose-per-air kerma factors allows independent evaluation of these quantities and provides possibility to choose most efficient Monte Carlo techniques for their computation. In the present work, computation of differential air kerma was performed in photon-only mode of radiation transport simulation, assuming secondary electron equilibrium conditions (also known as 'kerma approximation'). In contrast, absorbed doses in the tissue-equivalent spheres were computed using detailed physics and coupled electron-photon mode of transport simulation, accounting for transport of secondary photons and electrons as well as energy losses via bremsstrahlung.

Direct computation of differential air kerma results in accurate values of kerma integrals in the defined energy bins. These values are free from averaging errors, which would be unavoidable in case of scoring differential fluence with subsequent multiplication by bin-averaged mass-energy transfer coefficients and energy values. The second computed quantity – absorbed dose-per-air kerma coefficient – does not vary much within the considered energy bins, resulting in small uncertainties caused by averaging. Thus, the product of both quantities bears only modest uncertainties due to averaging dose-per-kerma values in the energy bins.

Use of spherical shapes for modelling bodies of various organisms, many of those being non-spherical, unavoidably introduces some uncertainties of the modelled DCC and limits applicability of the presented approach to assessment of average absorbed doses in the whole body. Realistic representation of the body shape and its internal structure as well as irradiation geometry might be important when dosimetric endpoints are absorbed doses in particular organs or exposure conditions suggest highly anisotropic irradiation of a static or slowly moving organism. If, however, the study endpoint is average absorbed dose in the whole body exposed in highly variable environmental conditions as is investigated in the present work, then the absorbed dose-per-air kerma coefficients for simple spheres provide a reasonable approximation. An example is shown in Fig. 5, where absorbed dose-per-air kerma values for a 70-kg sphere (closed circles) and for a 70-kg ellipsoid with extensions 167.2×40×20 cm (closed diamonds) are compared to effective dose-per-kerma values from a recent ICRP publication (ICRP 2011) for ROT- and ISO-fields (open squares and circles, respectively). All

response curves in the figure are remarkably similar and it is obvious that the effect of non-spherical body shape is small.

[Fig. 5 is about here]

The data obtained in the present study and the suggested technique provide plausible and robust DCC estimates for biological objects, mainly non-human biota, exposed to gamma radiation sources in radioactively contaminated soil. Interpolations for source photon energies, heights above ground, and body masses allow assessment of DCC for arbitrary values in the considered parameter ranges. The uncertainties inherent to the suggested technique are deemed to be less than other uncertainties which may originate from variability of environmental contamination, movement and migration of animals, seasonal variations of air kerma due to snow cover shielding or varying moisture content in soil, shielding by vegetation, and others.

Conclusions

The technique presented here was developed for calculation of DCC values, for external exposure of terrestrial biota, including birds and insects. In particular, it can be used to calculate DCC

- for body masses ranging from 10^{-6} to 10^{3} kg, thus closing the existing 'gap' in the current ICRP dosimetric approaches for terrestrial biota;
- for three environmental sources: an 'effective' plane source at depth 0.5 g cm^{-2}, a volume 'aged' source uniformly distributed in the upper 10 cm of soil, and an infinitely deep and uniformly distributed volume source in soil suitable for NORM;
- for heights above ground from 0.1 to 500 m;
- for energies of source photons ranging from 10 keV to 10 MeV, thus including the range of photon energies of all nuclides considered in the recent ICRP Publication 107 (ICRP, 2008b)

A number of simplifying assumptions have been used in the present study. First, an idealized 'infinite' flat source of uniform density has been selected for the modelling. Variations of soil properties and source distributions within the soil are known to cause some

variations of the gamma-radiation field above contaminated ground. Accounting for such variations can be important in applications related to *in-situ* gamma-spectrometry, but such effects are apparently less significant for the calculation of doses produced by both direct and scattered radiation. Nevertheless, studies of the influence of variations of soil and terrain properties on dose rates above ground are regarded as a useful source of information on environmental dose uncertainties, including the effects of uniform depth distributions typical for radionuclides of primordial origin.

Another simplifying assumption used in the present study was that only three types of sources in soil have been considered, ranging from planar to infinitely deep ones. However, the methodology described in the present paper can be further generalized and extended by computing air kerma spectra for 'elementary' plane sources at various depths, similarly to those computed and presented in (Eckerman and Ryman 1993). Air kerma spectra for such 'elementary' sources can be then interpolated, thus allowing folding them over any desired shape of depth distribution of activity in soil.

Finally, absorbed dose-to-air kerma ratios have been calculated for homogeneous spheres in an isotropic photon field. Homogeneity of target body, both in elemental composition and density, is a plausible assumption for radiation fields at high altitudes and for high photon energies. Use of isotropic radiation field for calculation of whole body doses (as it was done in the present study) can be particularly justified for organisms which move and change their location in the environment. Assumption of spherical body shape results in somewhat conservative DCC estimates, if the mean free paths of the incident photons are comparable to or larger than the body size, i.e. when the body appears 'transparent' to gamma-radiation. Alternatively, for lower energy photons and/or larger body masses, when the photon mean free paths are significantly shorter than the body size ('opaque' body), the dose response for spherical shapes becomes smaller than that for realistic shapes (see Fig. 5). Detailed investigations of dose responses for tissue-equivalent bodies of realistic shapes as compared to those of spherical shape might become the subject of another study.

References

Beck H, de Planque G (1968) The Radiation Field in Air due to distributed Gamma-ray Sources in the Ground. Report HASL-195. Health and Safety Laboratory. US Atomic Energy Comission, New York.

Bell GI, Glasstone S (1970) Nuclear Reactor Theory. Van Nostrand Reinhold Company, New York.

Brown JE, Alfonso B, Avila R, Beresford NA, Copplestone D, Pröhl G, Ulanovsky A (2008) The ERICA Tool. J Environ Radioactivity 99(9):1371–1383.

Eckerman KF, Ryman JC (1993) External exposure to radionuclides in air, water, and soil. Federal Guidance Report No. 12. EPA-402-R-93-081. US Environmental Protection Agency, Washington, DC.

ICRP (1996) Conversion Coefficients for use in Radiological Protection against External Radiation. ICRP Publication 74. Ann ICRP 26(3–4).

ICRP (2007) The 2007 Recommendations of the International Commission on Radiological Protection. ICRP Publication 103. Ann. ICRP 37(2–4).

ICRP (2008a) Environmental Protection – the Concept and Use of Reference Animals and Plants. ICRP Publication 108. Ann. ICRP 38(4–6).

ICRP (2008b) Nuclear Decay Data for Dosimetric Calculations. ICRP Publication 107. Ann. ICRP 38 (3).

ICRP (2011) Conversion Coefficients for Radiological Protection Quantities for External Radiation Exposures. ICRP Publication 116, Ann. ICRP 40(2–5).

ICRU (1989) Tissue Substitutes in Radiation Dosimetry and Measurement, Report 44 of the International Commission on Radiation Units and Measurements (Bethesda, MD).

ICRU (2011) Fundamental Quantities and Units for Ionizing Radiation (Revised). Report 85 of the International Commission on Radiation Units and Measurements. Journal of the ICRU 11(1).

Jacob P, Paretzke H (1986) Gamma-Ray Exposure from Contaminated Soil. Nucl Sci Engineering 93(3):248-261.

Hillmann U, Schimmack W, Jacob P, Bunzl K (1996) In situ gamma-spectrometry several years after deposition of radiocesium. Part I. Approximation of depth distributions by the Lorentz function. Radiat Environ Biophys 35(4):297–303.

LANL X-5 MONTE CARLO TEAM (2003) MCNP—A General Monte Carlo N-Particle Transport Code, Version 5. Volume I. MCNP Overview and Theory. LANL Report LA-UR-03-1987, Los Alamos National Laboratory.

Saito K, Jacob P (1995) Gamma Ray Fields in the Air due to Sources in the Ground. Radiat Prot Dosim 58(1):29–45.

Saito K, Ishigure N, Petoussi-Henss N, Schlattl H (2012) Effective dose conversion coefficients for radionuclides exponentially distributed in the ground. Radiat Environ Biophys 51:411–423.

Taranenko V, Pröhl G, Gómez-Ros JM (2004) Absorbed dose rate conversion coefficients for reference terrestrial biota for external photon and internal exposures. J Radiol Protect 24(4A):A35–A62.

Ulanovsky A, Pröhl G (2006) A practical method for assessment of dose conversion coefficients for aquatic biota. Radiat Environ Biophys 45:203–214.

Ulanovsky A, Pröhl G, Gómez-Ros JM (2008) Methods for calculating dose conversion coefficients for terrestrial and aquatic biota. J Environ Radioact 99(9):1440–1448.

Ulanovsky A, Pröhl G (2008) Tables of dose conversion coefficients for estimating internal and external radiation exposures to terrestrial and aquatic biota. Radiat Environ Biophys 47:195–203.

Figure captions

Fig. 1 Differential kerma in air at various heights above an infinite plane source of 10 MeV photons located in soil at a depth 0.5 g cm^{-2}

Fig. 2 Differential air kerma in air at various heights above a uniform source of 1 MeV photons located in the upper 10-cm-thick soil layer

Fig. 3 Comparison of air kerma spectra at various heights above the ground interface, for a planar and a 10-cm-thick volume source in soil emitting 0.5-MeV-photons

Fig. 4 Average absorbed dose per air kerma conversion factors (Gy Gy^{-1}) for tissue-equivalent spheres of various masses in an isotropic field of monoenergetic photons

Fig. 5 Comparison of dose-per-kerma ratios (Gy Gy^{-1}) for a tissue-equivalent 70-kg sphere and a 70-kg ellipsoid in an isotropic field of mono-energetic photons (this work) with effective dose per air kerma (Sv Gy^{-1}) for adult human in ROT and ISO external photons fields (ICRP 2011)

402 **Table 1** Elemental composition of materials used in the present work
403

Element	Z	Weight fraction (%)		
		Soil [a]	Air [a]	Tissue [b]
H	1	2.1	0.064	10.1
C	6	1.6	0.0124	11.1
N	7	57.7	75.5268	2.6
O	8	5.0	23.1781	76.2
Al	13	27.1		
Si	14	27.1		
Ar	18		1.281	
K	19	1.3		
Ca	20	4.1		
Fe	26	1.1		

[a] Eckerman and Ryman (1993)
[b] ICRU (1989)

404
405

406 **Table 2** Average absorbed dose rates per unit source strength of parent nuclide (μGy h^{-1}
407 Bq^{-1} m^2) in tissue-equivalent spheres at various heights above a planar source located at depth
408 0.5 g cm^{-2} in soil, for various radionuclides of anthropogenic origin.
409

Nuclide (progeny [a])	Mass (kg)				
	0.001	1	70	100	1000
			H = 1 m		
^{57}Co	3.3×10^{-7}	3.2×10^{-7}	2.3×10^{-7}	2.2×10^{-7}	1.2×10^{-7}
^{60}Co	6.9×10^{-6}	7.8×10^{-6}	6.5×10^{-6}	6.3×10^{-6}	4.3×10^{-6}
^{95}Zr (^{95m,95}Nb)	2.5×10^{-6}	2.5×10^{-6}	2.0×10^{-6}	1.9×10^{-6}	1.2×10^{-6}
^{131}I (^{131m}Xe)	1.3×10^{-6}	1.3×10^{-6}	9.8×10^{-7}	9.3×10^{-7}	5.6×10^{-7}
^{132}I	7.2×10^{-6}	7.4×10^{-6}	5.9×10^{-6}	5.6×10^{-6}	3.6×10^{-6}
^{134}Cs	5.4×10^{-6}	5.4×10^{-6}	4.3×10^{-6}	4.1×10^{-6}	2.6×10^{-6}
^{137}Cs (^{137m}Ba)	2.2×10^{-6}	2.1×10^{-6}	1.7×10^{-6}	1.6×10^{-6}	1.0×10^{-6}
^{152}Eu	3.4×10^{-6}	3.6×10^{-6}	2.9×10^{-6}	2.8×10^{-6}	1.8×10^{-6}
^{241}Am (^{237}Np)	7.1×10^{-8}	6.2×10^{-8}	3.6×10^{-8}	3.3×10^{-8}	1.7×10^{-8}
^{239}Pu (^{235m}U)	1.1×10^{-9}	4.6×10^{-10}	2.2×10^{-10}	2.0×10^{-10}	1.1×10^{-10}
			H = 10 m		
^{57}Co	2.9×10^{-7}	2.7×10^{-7}	2.0×10^{-7}	1.9×10^{-7}	1.1×10^{-7}
^{60}Co	5.7×10^{-6}	6.4×10^{-6}	5.4×10^{-6}	5.2×10^{-6}	3.5×10^{-6}
^{95}Zr (^{95m,95}Nb)	2.1×10^{-6}	2.1×10^{-6}	1.7×10^{-6}	1.6×10^{-6}	10.0×10^{-7}
^{131}I (^{131m}Xe)	1.1×10^{-6}	1.1×10^{-6}	8.1×10^{-7}	7.7×10^{-7}	4.6×10^{-7}
^{132}I	6.0×10^{-6}	6.1×10^{-6}	4.8×10^{-6}	4.6×10^{-6}	3.0×10^{-6}
^{134}Cs	4.5×10^{-6}	4.5×10^{-6}	3.5×10^{-6}	3.4×10^{-6}	2.1×10^{-6}
^{137}Cs (^{137m}Ba)	1.8×10^{-6}	1.8×10^{-6}	1.4×10^{-6}	1.3×10^{-6}	8.2×10^{-7}
^{152}Eu	2.9×10^{-6}	3.0×10^{-6}	2.4×10^{-6}	2.3×10^{-6}	1.5×10^{-6}
^{241}Am (^{237}Np)	6.0×10^{-8}	5.3×10^{-8}	3.0×10^{-8}	2.8×10^{-8}	1.5×10^{-8}
^{239}Pu (^{235m}U)	7.6×10^{-10}	3.4×10^{-10}	1.7×10^{-10}	1.6×10^{-10}	8.6×10^{-11}
			H = 500 m		
^{57}Co	2.0×10^{-8}	1.9×10^{-8}	1.2×10^{-8}	1.1×10^{-8}	6.1×10^{-9}
^{60}Co	8.1×10^{-7}	8.5×10^{-7}	6.8×10^{-7}	6.5×10^{-7}	4.3×10^{-7}
^{95}Zr (^{95m,95}Nb)	2.4×10^{-7}	2.3×10^{-7}	1.7×10^{-7}	1.7×10^{-7}	1.0×10^{-7}
^{131}I (^{131m}Xe)	1.1×10^{-7}	1.0×10^{-7}	7.5×10^{-8}	7.1×10^{-8}	4.1×10^{-8}
^{132}I	7.1×10^{-7}	7.0×10^{-7}	5.4×10^{-7}	5.1×10^{-7}	3.2×10^{-7}
^{134}Cs	5.3×10^{-7}	5.1×10^{-7}	3.9×10^{-7}	3.7×10^{-7}	2.2×10^{-7}
^{137}Cs (^{137m}Ba)	2.0×10^{-7}	2.0×10^{-7}	1.5×10^{-7}	1.4×10^{-7}	8.4×10^{-8}
^{152}Eu	3.5×10^{-7}	3.5×10^{-7}	2.7×10^{-7}	2.6×10^{-7}	1.7×10^{-7}
^{241}Am (^{237}Np)	1.1×10^{-9}	9.8×10^{-10}	5.2×10^{-10}	4.8×10^{-10}	2.5×10^{-10}
^{239}Pu (^{235m}U)	1.4×10^{-11}	1.3×10^{-11}	8.3×10^{-12}	7.8×10^{-12}	4.4×10^{-12}

[a] Relative activity of the progeny is expressed as integral activity within 15 days normalized to that of the parent nuclide

410
411
412

Table 3 Average absorbed dose rates per unit source strength of parent nuclide (μGy h^{-1} Bq^{-1} kg) in tissue-equivalent spheres at various heights above a 10-cm-thick volume source in soil, for various radionuclides of anthropogenic origin

Nuclide (progeny [a])	Mass (kg)				
	0.001	1	70	100	1000
			H = 1 m		
^{57}Co	1.7×10^{-5}	1.6×10^{-5}	1.1×10^{-5}	1.1×10^{-5}	6.1×10^{-6}
^{60}Co	4.5×10^{-4}	5.0×10^{-4}	4.1×10^{-4}	4.0×10^{-4}	2.7×10^{-4}
^{95}Zr (^{95m,95}Nb)	2.7×10^{-4}	2.7×10^{-4}	2.1×10^{-4}	2.0×10^{-4}	1.3×10^{-4}
^{131}I (^{131m}Xe)	8.1×10^{-5}	7.7×10^{-5}	5.8×10^{-5}	5.5×10^{-5}	3.3×10^{-5}
^{132}I	4.5×10^{-4}	4.6×10^{-4}	3.6×10^{-4}	3.5×10^{-4}	2.2×10^{-4}
^{134}Cs	3.4×10^{-4}	3.4×10^{-4}	2.6×10^{-4}	2.5×10^{-4}	1.6×10^{-4}
^{137}Cs (^{137m}Ba)	1.3×10^{-4}	1.3×10^{-4}	1.0×10^{-4}	9.7×10^{-5}	6.1×10^{-5}
^{152}Eu	2.2×10^{-4}	2.2×10^{-4}	1.8×10^{-4}	1.7×10^{-4}	1.1×10^{-4}
^{241}Am (^{237}Np, ^{233}Pa)	2.0×10^{-6}	1.8×10^{-6}	1.0×10^{-6}	9.3×10^{-7}	4.9×10^{-7}
^{239}Pu (^{235m}U)	3.9×10^{-8}	1.8×10^{-8}	9.4×10^{-9}	8.8×10^{-9}	4.9×10^{-9}
			H = 10 m		
^{57}Co	1.6×10^{-5}	1.5×10^{-5}	1.1×10^{-5}	10.0×10^{-6}	5.6×10^{-6}
^{60}Co	4.2×10^{-4}	4.6×10^{-4}	3.8×10^{-4}	3.7×10^{-4}	2.4×10^{-4}
^{95}Zr (^{95m,95}Nb)	2.5×10^{-4}	2.5×10^{-4}	1.9×10^{-4}	1.8×10^{-4}	1.2×10^{-4}
^{131}I (^{131m}Xe)	7.4×10^{-5}	7.0×10^{-5}	5.3×10^{-5}	5.0×10^{-5}	3.0×10^{-5}
^{132}I	4.2×10^{-4}	4.2×10^{-4}	3.3×10^{-4}	3.2×10^{-4}	2.0×10^{-4}
^{134}Cs	3.1×10^{-4}	3.1×10^{-4}	2.4×10^{-4}	2.3×10^{-4}	1.4×10^{-4}
^{137}Cs (^{137m}Ba)	1.2×10^{-4}	1.2×10^{-4}	9.3×10^{-5}	8.9×10^{-5}	5.5×10^{-5}
^{152}Eu	2.0×10^{-4}	2.1×10^{-4}	1.6×10^{-4}	1.6×10^{-4}	1.0×10^{-4}
^{241}Am (^{237}Np, ^{233}Pa)	1.7×10^{-6}	1.6×10^{-6}	8.9×10^{-7}	8.2×10^{-7}	4.3×10^{-7}
^{239}Pu (^{235m}U)	2.2×10^{-8}	1.3×10^{-8}	7.8×10^{-9}	7.3×10^{-9}	4.1×10^{-9}
			H = 500 m		
^{57}Co	1.3×10^{-6}	1.3×10^{-6}	8.1×10^{-7}	7.5×10^{-7}	4.1×10^{-7}
^{60}Co	8.7×10^{-5}	9.1×10^{-5}	7.2×10^{-5}	6.9×10^{-5}	4.5×10^{-5}
^{95}Zr (^{95m,95}Nb)	4.0×10^{-5}	3.9×10^{-5}	3.0×10^{-5}	2.8×10^{-5}	1.7×10^{-5}
^{131}I (^{131m}Xe)	1.0×10^{-5}	9.5×10^{-6}	6.8×10^{-6}	6.4×10^{-6}	3.8×10^{-6}
^{132}I	7.2×10^{-5}	7.1×10^{-5}	5.4×10^{-5}	5.1×10^{-5}	3.2×10^{-5}
^{134}Cs	5.3×10^{-5}	5.1×10^{-5}	3.9×10^{-5}	3.7×10^{-5}	2.2×10^{-5}
^{137}Cs (^{137m}Ba)	2.0×10^{-5}	2.0×10^{-5}	1.5×10^{-5}	1.4×10^{-5}	8.3×10^{-6}
^{152}Eu	3.6×10^{-5}	3.6×10^{-5}	2.8×10^{-5}	2.7×10^{-5}	1.7×10^{-5}
^{241}Am (^{237}Np, ^{233}Pa)	4.3×10^{-8}	3.8×10^{-8}	2.0×10^{-8}	1.8×10^{-8}	9.4×10^{-9}
^{239}Pu (^{235m}U)	1.1×10^{-9}	1.0×10^{-9}	6.7×10^{-10}	6.3×10^{-10}	3.6×10^{-10}

[a] Relative activity of the progeny is expressed as integral activity within 1 year normalized to that of the parent nuclide

Table 4 Average absorbed dose rates per unit source strength of parent nuclide (μGy h^{-1} Bq^{-1} kg) in tissue-equivalent spheres at various heights above an infinitely deep volume source in soil, for radionuclides of primordial origin

Nuclide(s)	Mass (kg)				
	0.001	1	70	100	1000
H = 1 m					
^{40}K	3.7×10^{-5}	4.2×10^{-5}	3.5×10^{-5}	3.3×10^{-5}	2.3×10^{-5}
^{235}U-series [a]	1.5×10^{-4}	1.4×10^{-4}	1.1×10^{-4}	9.9×10^{-5}	5.8×10^{-5}
^{238}U-series [a]	2.4×10^{-4}	2.7×10^{-4}	2.2×10^{-4}	2.1×10^{-4}	1.4×10^{-4}
^{232}Th-series [a]	5.8×10^{-4}	6.7×10^{-4}	5.5×10^{-4}	5.3×10^{-4}	3.6×10^{-4}
H = 10 m					
^{40}K	3.5×10^{-5}	3.9×10^{-5}	3.2×10^{-5}	3.1×10^{-5}	2.1×10^{-5}
^{235}U-series [a]	1.4×10^{-4}	1.3×10^{-4}	9.6×10^{-5}	9.1×10^{-5}	5.3×10^{-5}
^{238}U-series [a]	2.3×10^{-4}	2.5×10^{-4}	2.0×10^{-4}	1.9×10^{-4}	1.3×10^{-4}
^{232}Th-series [a]	5.4×10^{-4}	6.3×10^{-4}	5.2×10^{-4}	5.0×10^{-4}	3.4×10^{-4}
H = 100 m					
^{40}K	2.4×10^{-5}	2.6×10^{-5}	2.1×10^{-5}	2.0×10^{-5}	1.3×10^{-5}
^{235}U-series [a]	8.2×10^{-5}	7.8×10^{-5}	5.6×10^{-5}	5.2×10^{-5}	3.0×10^{-5}
^{238}U-series [a]	1.5×10^{-4}	1.6×10^{-4}	1.3×10^{-4}	1.2×10^{-4}	8.1×10^{-5}
^{232}Th-series [a]	3.6×10^{-4}	4.2×10^{-4}	3.4×10^{-4}	3.3×10^{-4}	2.2×10^{-4}
H = 500 m					
^{40}K	8.4×10^{-6}	8.9×10^{-6}	7.2×10^{-6}	6.9×10^{-6}	4.5×10^{-6}
^{235}U-series [a]	1.8×10^{-5}	1.7×10^{-5}	1.2×10^{-5}	1.1×10^{-5}	6.2×10^{-6}
^{238}U-series [a]	5.0×10^{-5}	5.3×10^{-5}	4.2×10^{-5}	4.0×10^{-5}	2.6×10^{-5}
^{232}Th-series [a]	1.3×10^{-4}	1.5×10^{-4}	1.2×10^{-4}	1.2×10^{-4}	8.1×10^{-5}

[a] Accounted progeny is assumed in secular equilibrium with parent

FIGURES

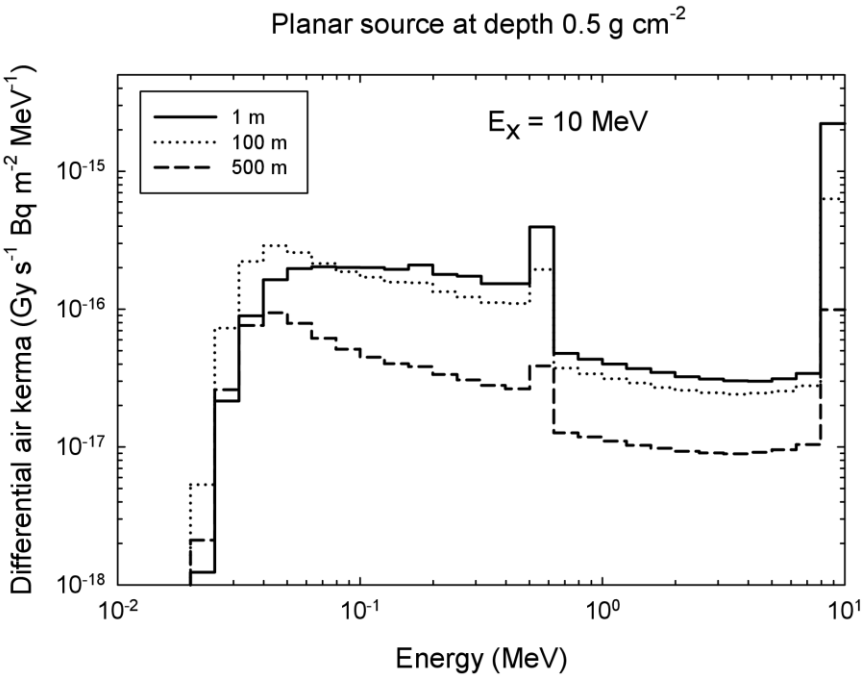

Fig. 1

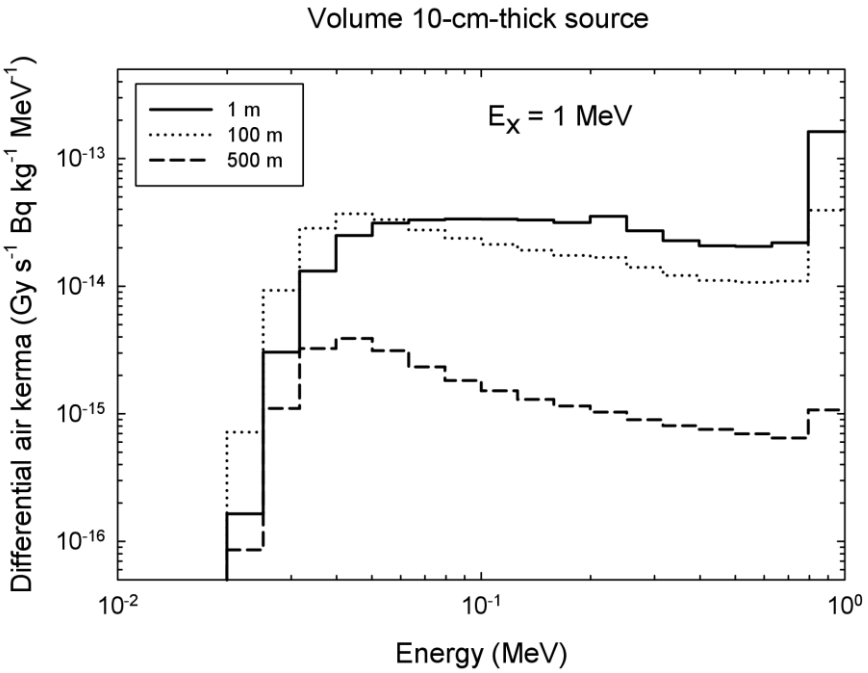

Fig. 2

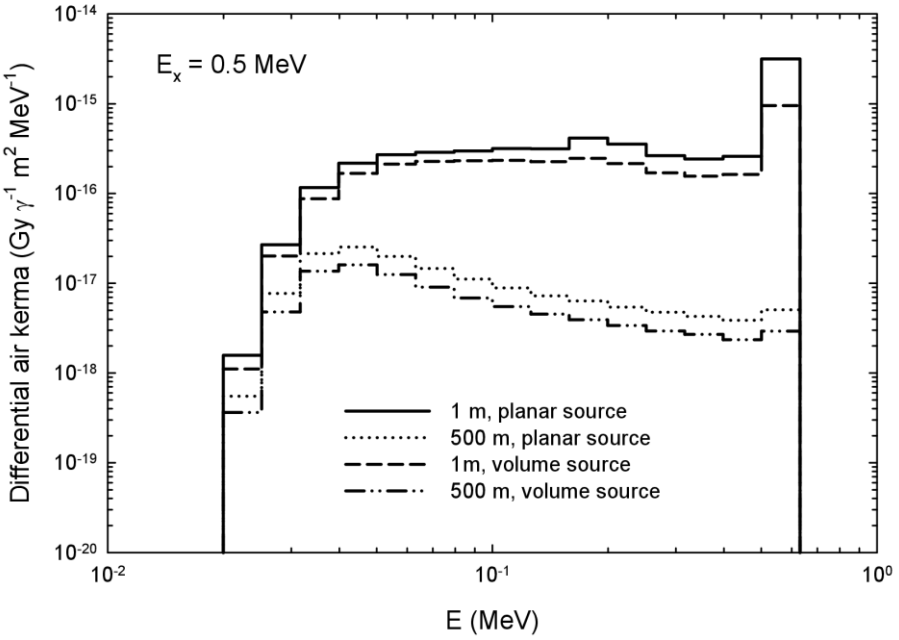

435
436 **Fig. 3**
437
438

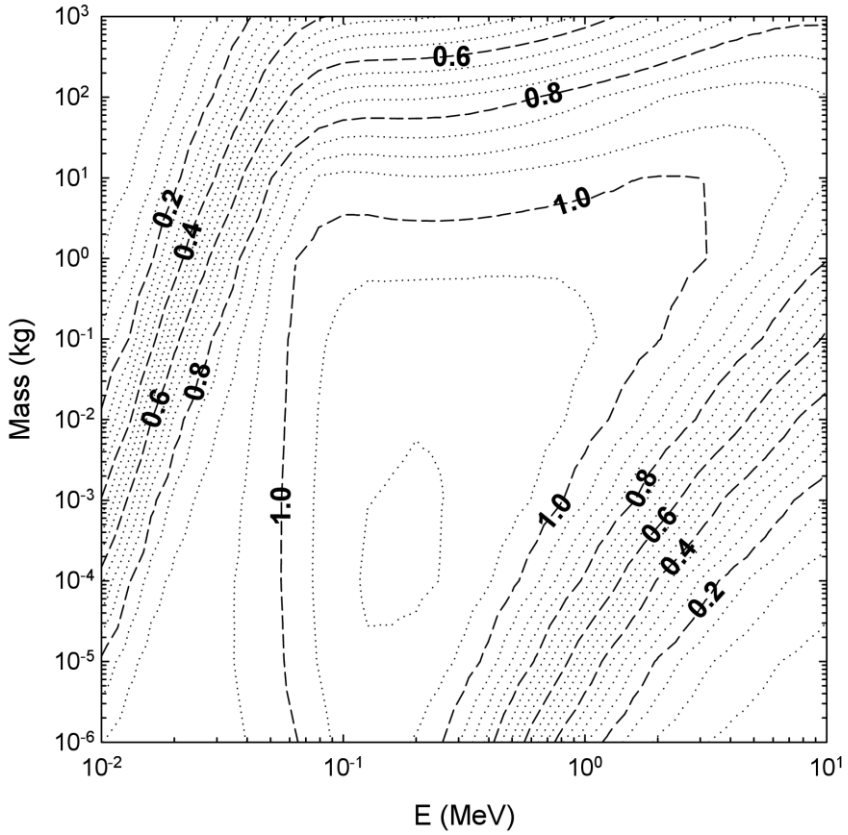

439
440 **Fig. 4**
441

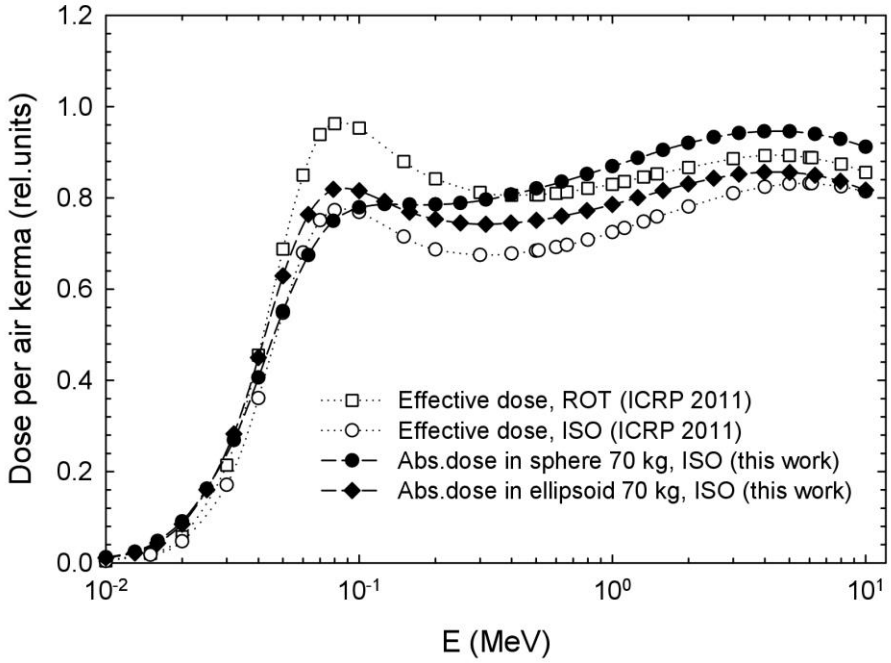
Dose per air kerma (rel.units)
E (MeV)
Effective dose, ROT (ICRP 2011)
Effective dose, ISO (ICRP 2011)
Abs.dose in sphere 70 kg, ISO (this work)
Abs.dose in ellipsoid 70 kg, ISO (this work)

Fig. 5